METABOLISM

Hypothalamic Ventromedial Lin28a Enhances Glucose Metabolism in Diet-Induced Obesity

Jung Dae Kim,[1,2] Chitoku Toda,[1,2] Cristina M. Ramírez,[2,3] Carlos Fernández-Hernando,[2,3] and Sabrina Diano[1,2,3,4]

The Lin28a/*Let-7* axis has been studied in peripheral tissues for its role in metabolism regulation. However, its central function remains unclear. Here we found that Lin28a is highly expressed in the hypothalamus compared with peripheral tissues. Its expression is positively correlated with positive energy balance, suggesting a potential central role for Lin28a in metabolism regulation. Thus, we targeted the hypothalamic ventromedial nucleus (VMH) to selectively overexpress (*Lin28aKI^VMH*) or downregulate (*Lin28aKD^VMH*) Lin28a expression in mice. With mice on a standard chow diet, body weight and glucose homeostasis were not affected in *Lin28aKI^VMH* or *Lin28aKD^VMH* mice. On a high-fat diet, although no differences in body weight and composition were observed, *Lin28aKI^VMH* mice showed improved glucose tolerance and insulin sensitivity compared with controls. Conversely, *Lin28aKD^VMH* mice displayed glucose intolerance and insulin resistance. Changes in VMH AKT activation of diet-induced obese *Lin28aKI^VMH* or *Lin28aKD^VMH* mice were not associated with alterations in *Let-7* levels or insulin receptor activation. Rather, we observed altered expression of TANK-binding kinase-1 (TBK-1), which was found to be a direct Lin28a target mRNA. VMH-specific inhibition of TBK-1 in mice with diet-induced obesity impaired glucose metabolism and AKT activation. Altogether, our data show a TBK-1–dependent role for central Lin28a in glucose homeostasis.

Control of gene expression is important for many functions during both development and adulthood. Lin28a is an RNA-binding protein that has been shown to selectively repress the expression of microRNAs (miRNAs), including those belonging to the *Let-7* family (1,2). *Let-7* miRNA family members act as suppressors of numerous genes involved in the insulin signaling pathway including IGF1R, INSR, IRS2, PIK3IP1, AKT2, TSC1, and RICTOR (3,4). In accordance with these findings, it has been recently reported that whole-body Lin28a transgenic mice have reduced muscle *Let-7* expression (4) that was associated with improved glucose tolerance and insulin sensitivity (4). Conversely, skeletal muscle and brown adipose tissue (BAT)-specific Lin28a knockout mice displayed impaired glucose tolerance and insulin resistance (5), although no changes in muscle *Let-7* levels were observed (5). Furthermore, whole-body and pancreas-specific overexpression of *Let-7* in mice resulted in impaired glucose tolerance and reduced glucose-induced insulin secretion. Tissue-specific knockdown of *Let-7* in *Let-7* transgenic mice reversed the phenotype by improving insulin sensitivity in the muscle and adipose tissues (3). Although these observations strongly suggest a role for the Lin28a/*Let-7* axis in controlling glucose homeostasis, how its expression in the central nervous system influences glucose metabolism has not been evaluated (3–5).

In the central nervous system, the hypothalamus plays an essential role in the homeostatic control of circulating glucose levels by altering hepatic glucose production and utilization in peripheral tissues (6,7) and by regulating pancreatic secretion of hormones, including insulin (8). The ventromedial nucleus of the hypothalamus (VMH) has been shown to control energy and glucose homeostasis (9–11). Neurons in the VMH express numerous receptors for circulating hormones, including insulin. When insulin activates its receptor, the cytoplasmic tail is phosphorylated

---

[1]Department of Obstetrics, Gynecology, and Reproductive Sciences, Yale University School of Medicine, New Haven, CT

[2]Department of Comparative Medicine, Yale University School of Medicine, New Haven, CT

[3]Program in Cell Signaling and Neurobiology of Metabolism, Yale University School of Medicine, New Haven, CT

[4]Department of Neuroscience, Yale University School of Medicine, New Haven, CT

Corresponding author: Sabrina Diano, sabrina.diano@yale.edu.

in a tyrosine residue, allowing the recruitment of IRS proteins and facilitating the activation of downstream effectors, such as phosphatidylinositol 3-kinase (PI3K) and mitogen-activated protein kinase (MAPK). The primary signaling pathway regulated by IRS proteins is the PI3K–protein kinase B (PKB/AKT) cascade, which controls the activation of downstream effectors including glycogen synthase kinase 3β (GSK3β), mammalian target of rapamycin complex 1 (mTORC1) and mTORC2, and Forkhead transcription factors (12). For assessment of whether central Lin28 plays a role in the regulation of energy and glucose homeostasis, the following studies were performed.

RESEARCH DESIGN AND METHODS

Animal Care

C57BL/6 (stock no. 000664) and Lin28a floxed (Lin28a$^{f/f}$ [stock no. 023913]) mice were purchased from The Jackson Laboratory. All animal care and experimental procedures performed in this study were approved by the Yale University Institutional Animal Care and Use Committee. Animals (age 2–4 months) were provided a standard chow diet (SD) (diet no. 2018; 18% calories from fat; Teklad Diets, Harlan Laboratories) or high-fat diet (HFD) (category no. 93075; 45% fat; Teklad Diets, Harlan Laboratories) and water ad libitum unless otherwise stated.

Western Blot

Protein lysates of peripheral tissues and hypothalamus (or punched arcuate nucleus [ARC], VMH, and dorsomedial nucleus of the hypothalamus [DMH]) were prepared as previously described (8,13). The following antibodies were used: anti-AKT (category no. 9272; Cell Signaling Technology), anti–phosphorylated (p-) AKT (4058; Cell Signaling Technology), anti–insulin receptor (IR) (3025; Cell Signaling Technology), anti–p-IR (44800G; Invitrogen), anti-S6K1 (ab119252; Abcam), anti–p-S6K1 (ab32525; Abcam), anti–TANK-binding kinase-1 (TBK-1) (3013; Cell Signaling Technology), and anti-Lin28a (ab46020; Abcam). Membrane were developed using an ECL kit (32016; Thermo Fisher Scientific). Membranes were reused to detect β-actin (A5441; Sigma-Aldrich) or GAPDH (Sc-25778; Santa Cruz Biotechnology) after stripping with Restore PLUS Western Blot Stripping Buffer (46430; Thermo Fisher Scientific).

Adeno-Associated Virus Injection Into the VMH

Adeno-associated virus (AAV) vectors expressing Cre-GFP (category no. 7016, AAV2-Cre-GFP), Lin28a-GFP (AAV2-CMV-GFP-CMV-mLin28a, customized virus), and GFP (category no. 7004, AAV2-GFP) were purchased from Vector Biolabs and injected bilaterally into the VMH (coordinates, bregma: anterior-posterior, −1.5 mm; lateral, ±0.4 mm; and dorsal-ventral, −5.8 mm) at a rate of 40 nL/min (~1 × 10^{12} viral particles/mL) for 15 min, and the injector remained in place for an additional 5 min before removal.

GFP Immunostaining

Immunofluorescence staining was performed to confirm the injection site using anti-GFP antibody (ab13970; Abcam). Mice in which viral injections were located outside the VMH were studied separately. Brains were sectioned with a vibratome (50 μm), and sections were incubated overnight in anti-GFP antibody (diluted 1:5,000 in 0.1 mol/L sodium phosphate buffer) and then incubated in secondary antibody (category no. A11039, Alexa Fluor 488–coupled goat anti-chicken, 1:500 dilution; Life Technologies) for 2 h. Sections were then cover slipped with VECTASHIELD (H-1000; Vector Laboratories) for microscopic examination.

Glucose Tolerance Test, Insulin Tolerance Test, and MRI

Glucose tolerance tests (GTTs) were performed with 2 g/kg glucose (category no. G5765; Sigma-Aldrich) in animals fasted for 16–17 h as previously described (8,13). For insulin tolerance tests, animal received an injection of insulin (1 unit/kg i.p.; Actrapid, Novo Nordisk A/S Denmark) (8,13). For body composition, adult males were scanned in
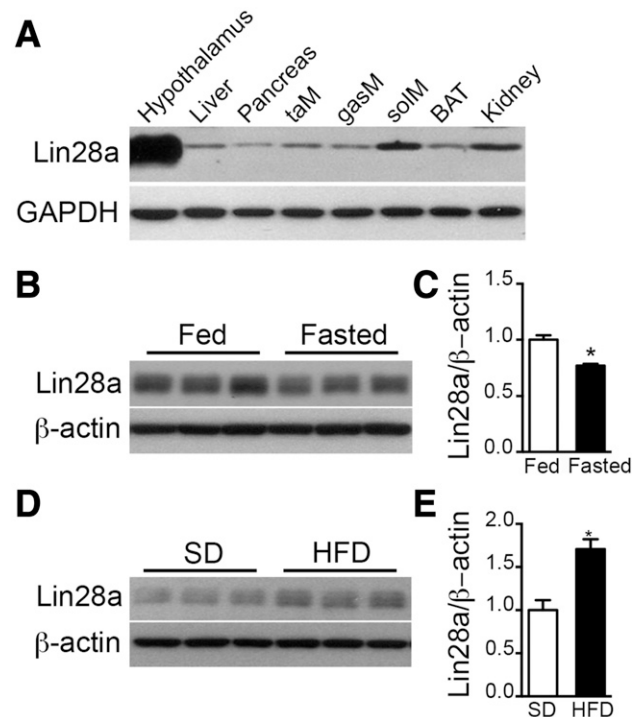

Figure 1—Lin28a is highly expressed in the hypothalamus and is metabolically regulated. A: Western blot analysis showing the relative expression levels of Lin28a in tissues including the hypothalamus, liver, pancreas, tibialis anterior muscle (taM), gastrocnemius muscle (gasM), soleus muscle (solM), BAT, and kidney. B: Representative Western blot image of Lin28a expression in hypothalamic samples from fed (n = 4) and overnight fasted (n = 3) mice. C: Graph of densitometry analysis of Lin28a showing a significant decrease of Lin28a after an overnight fast. D: Representative Western blot image of Lin28a expression in hypothalamic samples from mice exposed to an SD (n = 3) and 12 weeks of HFD (45% HFD) (n = 5). E: Graph of densitometry analysis of Lin28a showing a significant increase of Lin28a after HFD feeding. Data represent the mean ± SEM. *P < 0.05.

an EchoMRI machine (Echo Medical Systems, Houston, TX).

Insulin and Glucagon Measurement

Circulating insulin levels were analyzed by ELISA (category no. EZRMI-13K; EMD Millipore) according to the manufacture's protocol. Plasma glucagon was measured by ELISA (DGCG0; R&D Systems, Inc.) according to the manufacture's protocol.

Hyperinsulinemic-Euglycemic Clamp

The hyperinsulinemic-euglycemic clamp was performed as previously described (8,13). Briefly, the hyperinsulinemic-euglycemic clamp was initiated with the 90-min basal period (t = −90 to 0 min) followed by a 115-min clamp period (t = 0 to 115 min). The clamp period was initiated at t = 0 min by primed and continuous infusion of human insulin (2.5–1.25 mU · kg^{-1} · min^{-1}, Humulin R; Eli Lilly). A priming dose of [3-^{3}H]glucose (5 μCi) (Perkin Elmer) was administered at t = −90 min and was followed by infusion of the tracer at a rate of 0.05 μCi/min for 1.5 h. Glucose (30%) was infused at a variable rate to maintain blood glucose levels at 110–130 mg/dL. Tissue 2-[^{14}C]-deoxy-D-glucose uptake was also measured as previously described (8,13).

c-Fos Immunostaining

Mice were injected with 2 g/kg glucose i.p. in sterile saline at 9:00 A.M. after overnight fasting. Mice were perfused 45 min later with 4% paraformaldehyde, brains were dissected and sectioned at 50 μm, and c-Fos staining (diluted 1:2,000 in 0.1 mol/L phosphate buffer [category no. sc-52; Santa Cruz Biotechnology]) was performed and analyzed as previously described (8,13).

Total RNA Preparation and Real-time RT-PCR

Total RNA extraction and real-time PCR were performed as previously described (8,13) TaqMan Gene Expression Assay primers (Thermo Fisher Scientific) in a 10-μL reaction volume were used: Lin28a, Mm00524077_m1; TBK-1, Mm00451150_m1; RICTOR, Mm01307318_m1; β-actin, Mm02619580_g1; and GAPDH, Mm99999915_g1. For Let-7 miRNA measurement, total RNA was reverse transcribed using the miScript II RT Kit (Qiagen) following the manufacture's instructions. Specific primers for mouse Let-7 miRNAs (Let-7i, Let-7b, and Let-7d) were used and values normalized to SNORD68 (Qiagen) as a housekeeping gene.

RNA Immunoprecipitation

RNA immunoprecipitation (RIP) was performed using the Imprint RNA Immunoprecipitation Kit (RIP; Sigma-Aldrich) according to the manufacturer's instructions. In brief, 20 μL magnetic beads was preincubated with 2 μg anti-Lin28a antibody (ab46020; Abcam) or 2 μg rabbit preimmune IgG in 100 μL RIP wash buffer for 30 min at room temperature, and then the magnetic beads were washed with RIP wash buffer and kept on ice until used. Hypothalamic protein lysates were prepared by mild lysis buffer including protease inhibitor cocktail and RNase inhibitor (40 units/μL) provided by Kit. After centrifugation, lysates were incubated with antibody or preimmune IgG prebound magnetic beads by rotation overnight at 4°C. The magnetic beads were washed and resuspended in 200 μL RIP wash buffer. For total RNA extraction, 500 μL TRIzol LS Reagent and 100 μL chloroform were added to each tube and centrifuged at 4°C for 10 min at 16,000g. Aqueous upper phase was
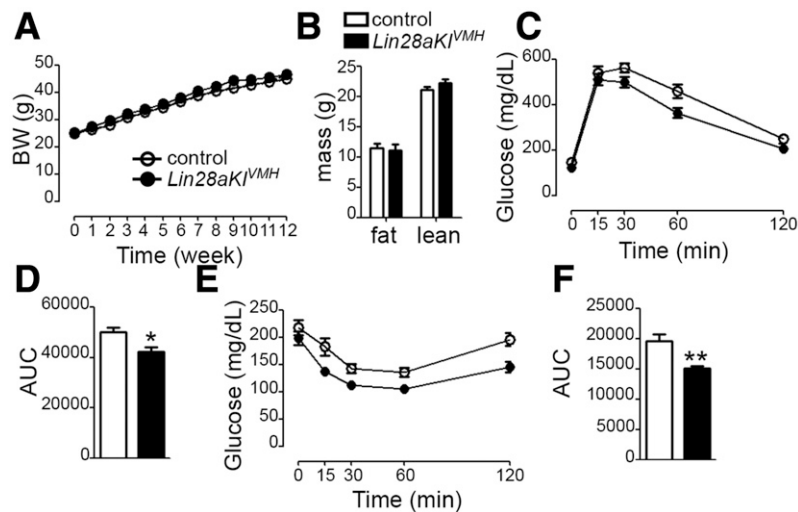

Figure 2—VMH-selective Lin28a overexpression improves glucose metabolism. *A* and *B*: Graphs showing body weight (BW) and body fat and lean mass in *Lin28aKI^{VMH}* mice (n = 8) and controls (n = 8) exposed to an HFD (45%). *C* and *D*: Graphs showing GTT (*C*) and the area under the curve (AUC) (*D*) in DIO *Lin28aKI^{VMH}* mice (n = 8) and controls (n = 8) after 8 weeks' exposure to an HFD (45%). *E* and *F*: Graphs showing insulin tolerance test (*E*) and the area under the curve (*F*) in DIO *Lin28aKI^{VMH}* mice (n = 8) and controls (n = 8) after 8 weeks' exposure to an HFD (45%). Data represent the mean ± SEM. *P < 0.05; **P < 0.01.
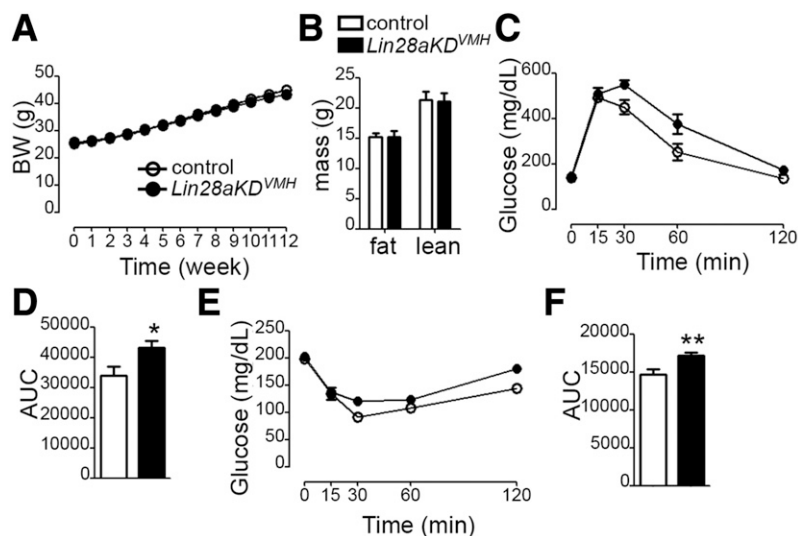
Figure 3—VMH-selective Lin28a downregulation impairs glucose metabolism. *A* and *B*: Graphs showing body weight (BW) and body fat and lean mass in *Lin28aKD*^VMH mice (*n* = 8) and controls (*n* = 8) exposed to an HFD (45%). *C* and *D*: Graphs showing GTT (*C*) and the area under the curve (AUC) (*D*) in DIO *Lin28aKD*^VMH mice (*n* = 8) and controls (*n* = 8) after 8 weeks' exposure to an HFD (45%). *E* and *F*: Graphs showing insulin tolerance test (*E*) and the area under the curve (*F*) in DIO *Lin28aKD*^VMH mice (*n* = 8) and controls (*n* = 8) after 8 weeks' exposure to an HFD (45%). Data represent the mean ± SEM. *$P < 0.05$; **$P < 0.01$.

transferred to a new tube, and 6 μL of linear acrylamide, 60 μL of 5 mol/L ammonium acetate, and 600 μL of 2-propanol were added. After 1 h incubation at −80°C, samples were centrifuged at 4°C for 20 min at 16,000*g* and rinsed with 80% ethanol. The pellets were resuspended in 20 μL RNase-free water and subjected to cDNA synthesis followed by real-time PCR as described above.

Inhibitor Administration Into the VMH

Bilateral cannula was implanted into the VMH (coordinates, bregma: anterior-posterior, −1.5 mm; lateral, ±0.4 mm; and dorsal-ventral, −5.75 mm). After a week of recovery, BX795 (10 ng/site in saline containing 0.1% DMSO at a rate of 0.1 μL/min, category no. ENZ-CHM189; Enzo Life Sciences, Inc.), LY294002 (100 ng/site in saline containing 1% DMSO at a rate of 0.1 μL/min, category no. TLRL-LY29;
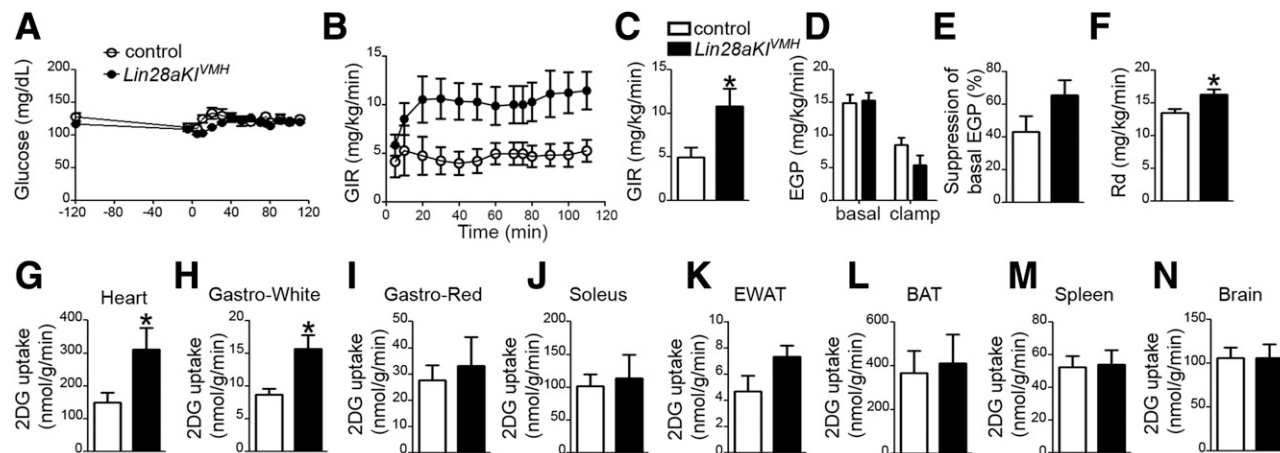

Figure 4—VMH-selective Lin28a overexpression improves peripheral glucose metabolism. *A*: Blood glucose levels during the basal and clamp periods in DIO *Lin28aKI*^VMH mice (*n* = 8) and control mice (*n* = 8) after 8 weeks on an HFD (45%). The clamp period begins at time 0. *B* and *C*: Graphs showing glucose infusion rate (GIR) required to maintain euglycemia during the clamp period. In panel *C*, the data are shown as the means of the values from 70 to 115 min. *D*: EGP during both basal and clamp periods. *E*: Graph showing the percentage suppression of basal EGP induced by insulin infusion. *F*: Graph showing the R_d during the clamp period, which represents whole-body glucose utilization. Basal R_d is equal to basal EGP. *G–N*: 2-[^{14}C]-deoxy-D-glucose (2DG) uptake in the heart (*G*), white (Gastro-White) (*H*) and red (Gastro-Red) (*I*) portions of the gastrocnemius, soleus (*J*), epididymal white adipose tissue (EWAT) (*K*), BAT (*L*), spleen (*M*), and brain (*N*) during the clamp period. All data represent mean ± SEM. *$P < 0.05$ (*n* = 7–8 male mice per group).

InvivoGen), rapamycin (2 ng/site in saline containing 0.1% DMSO at a rate of 0.1 μL/min, category no. 553210, Calbiochem), or the equivalent volume of vehicle (saline containing DMSO) was infused, and 50 min later GTT was performed as described above.

Statistical Analysis

Two-way ANOVA was used to determine the effect of the genotype and treatment with the Prism 4.0 software (GraphPad Software). For repeated-measures analysis, ANOVA was used when values over different times were analyzed. When only two groups were analyzed, statistical significance was determined by an unpaired Student t test. A value of $P < 0.05$ was considered statistically significant. All data are shown as mean ± SEM unless stated otherwise.

RESULTS

Lin28a Is Highly Expressed in the Hypothalamus and Is Metabolically Regulated

First, we determined the expression of Lin28a in the hypothalamus and a number of peripheral tissues by immunoblotting. Surprisingly, Lin28a was highly expressed in the hypothalamus compared with other metabolic tissues including liver, pancreas, BAT, kidney, and muscles (Fig. 1A). To assess whether Lin28a expression levels in the brain is affected by the metabolic state, we measured hypothalamic Lin28a expression in fed and fasted states and in mice with diet-induced obesity compared with SD-fed controls. The results showed that Lin28a expression was significantly reduced in the hypothalamus of fasted mice compared with fed animals (Fig. 1B and C). Moreover, Lin28 expression was significantly increased in the hypothalamus of mice with diet-induced obesity (DIO mice) compared with SD-fed mice (Fig. 1D and E).

Hypothalamic Lin28a Expression Influences Glucose Homeostasis in Mice on HFD

Previous reports have shown that Lin28a play a major role in controlling glucose homeostasis (4). Since the VMH is critical for peripheral glucose regulation (9–11), we hypothesized that hypothalamic Lin28a expression might play a role in regulating glucose metabolism. To test this notion, we selectively overexpressed or knockdown Lin28a expression in the VMH by VMH-targeted viral injections of either AAV-Lin28a-EGFP in C57Bl6 mice (to overexpress) or AAV-cre-GFP in $Lin28a^{f/f}$ mice (to inhibit). VMH targeting was confirmed by GFP immunostaining (Supplementary Fig. 1) and by immunoblot (Supplementary Fig. 2A, B, D, and E) and real-time PCR analysis (Supplementary Fig. 2C and F). When mice were exposed to SD, no differences in body weight or body composition and glucose tolerance or insulin sensitivity were observed between Lin28 VMH-overexpressing mice ($Lin28aKI^{VMH}$) and controls ($EGFP^{VMH}$) (Supplementary Fig. 3A–D) or Lin28a knockdown mice ($Lin28aKD^{VMH}$) and controls ($Lin28a^{EGFP/VMH}$) (Supplementary Fig. 3E–H). Similarly, when mice were fed an HFD, no differences in body weight or composition were observed

between either $Lin28aKI^{VMH}$ mice and controls (Fig. 2A and B) or $Lin28aKD^{VMH}$ mice and controls (Fig. 3A and B). However, HFD-fed $Lin28aKI^{VMH}$ mice showed improved glucose tolerance (Fig. 2C and D) and insulin sensitivity (Fig. 2E and F) compared with HFD-fed controls. Consistent with the $Lin28aKI^{VMH}$ data, HFD-fed $Lin28aKD^{VMH}$ mice showed glucose intolerance (Fig. 3C and D) and insulin resistance (Fig. 3E and F) compared with HFD-fed controls. No difference in fed (Supplementary Fig. 4A and B) or fasted (Supplementary Fig. 4C and D) insulin or glucagon levels were observed between $Lin28aKI^{VMH}$ mice and controls. Similar results were observed in $Lin28aKD^{VMH}$ mice and controls (Supplementary Fig. 4E–H).

Mice in which Lin28a-targeted viral delivery was mistakenly located outside the VMH, in the DMH (Supplementary Fig. 5A, B, E, and F), showed no glucose
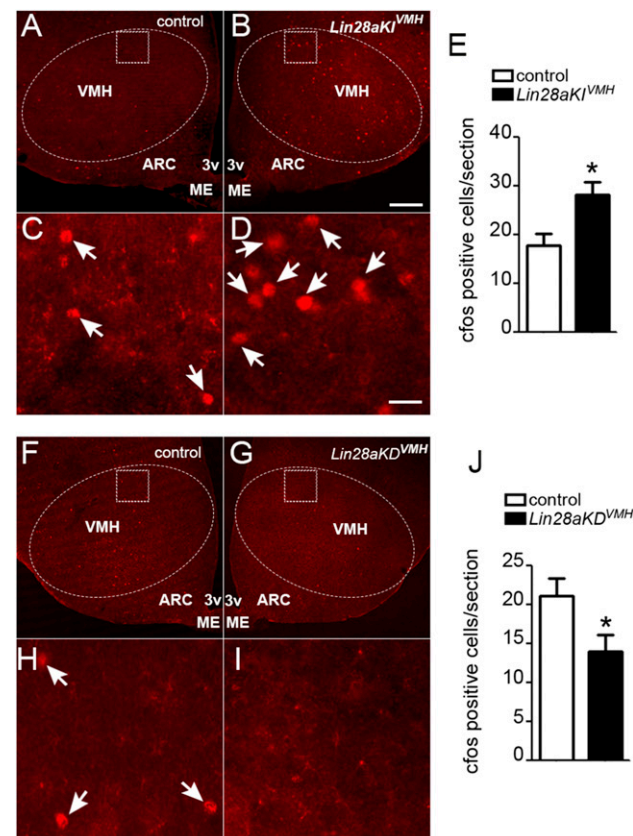

Figure 5—Lin28a affects VMH neuronal activation. A and B: Representative micrographs of hypothalamic sections from control (A) and $Lin28aKI^{VMH}$ (B) mice showing c-Fos staining. C and D: High-power magnifications of the VMH areas highlighted in A (for C) and B (for D). E: Graph showing the results of c-Fos counting in the VMH of control and $Lin28aKI^{VMH}$ mice (n = 5 DIO mice per group; 8 weeks on HFD). F and G: Representative micrographs of hypothalamic sections from control (F) and $Lin28aKD^{VMH}$ (G) mice showing c-Fos immunostaining. H and I: High-power magnifications of the VMH areas highlighted in F (for H) and G (for I). J: Graph showing the results of c-Fos counting in the VMH of control and $Lin28aKD^{VMH}$ mice (n = 5 DIO mice per group; 8 weeks on HFD). *$P < 0.05$. Arrows indicate c-Fos labeling in nuclei. ME, median eminence; 3v, third ventricle. Bar scale in B (for A, F, and G) represents 200 μm. Bar scale in D (for C, H, and I) represents 30 μm.

metabolic phenotype (Supplementary Fig. 5C, D, G, and H).

Next, we performed hyperinsulinemic-euglycemic clamp studies to assess insulin sensitivity in HFD-fed Lin28aKI^{VMH} and control mice. Higher glucose infusion rate was required to maintain euglycemia in Lin28aKI^{VMH} mice compared with control mice (Fig. 4A–C). Endogenous glucose production (EGP) was not statistically significant between the two groups (Fig. 4D and E). However, Lin28aKI^{VMH} mice showed increased glucose disappearance (R_d) during the clamp period (Fig. 4F), together with a greater glucose uptake in the heart (Fig. 4G) and the gastrocnemius white muscle (Fig. 4H), while no significant differences were found in the gastrocnemius red muscle (Fig. 4I), soleus (Fig. 4J), epididymal white adipose tissue (Fig. 4K), BAT (Fig. 4L), spleen (Fig. 4M), or brain (Fig. 4N).

Lin28a Expression Alters c-Fos Activation in the VMH

To assess whether Lin28a expression affected VMH neuronal activation in response to a glucose load, we then performed c-Fos staining after peripheral glucose administration. Glucose load to Lin28aKI^{VMH} mice induced a significant increase of c-Fos immunoreactivity in the VMH compared with control mice (Fig. 5A–E). Consistent with these data, when glucose was injected into Lin28aKD^{VMH} mice a significant reduction in c-Fos immunoreactivity

was observed compared with controls (Fig. 5F–J). No difference in c-Fos staining was observed in either the ARC or the DMH of the Lin28aKI^{VMH} (Supplementary Fig. 6A and B) or the Lin28aKD^{VMH} (Supplementary Fig. 6C and D) mice compared with their respective controls. Altogether, these data suggest that VMH Lin28a selectively affects VMH neuronal activation in response to a glucose load.

Lin28a Modulates AKT Pathway Independently From IRs

Lin28a has been shown to influence insulin signaling in peripheral tissues via the Lin28a/Let-7 axis. Lin28a regulates Let-7 levels, which regulates posttranscriptionally the expression of genes associated with the insulin-PI3K-mTOR pathway in a number of metabolic tissues such as muscle and pancreas (4). Therefore, to investigate the effect of Lin28a on insulin signaling pathway, we analyzed the phosphorylation levels of the IR-PI3K-AKT-mTOR pathway in the VMH of Lin28aKI^{VMH} and Lin28aKD^{VMH} mice compared with their respective controls. Interestingly, while no changes in the activation levels of IR were observed in either Lin28aKI^{VMH} (Fig. 6A and B) or Lin28aKD^{VMH} (Fig. 6E and F) mice compared with their respective controls, AKT and S6K1 phosphorylation levels were increased in Lin28aKI^{VMH} mice (Fig. 6A, C, and D) and decreased in Lin28aKD^{VMH} mice (Fig. 6E, G, and H) compared with their respective controls. Next, to assess whether Let-7 levels
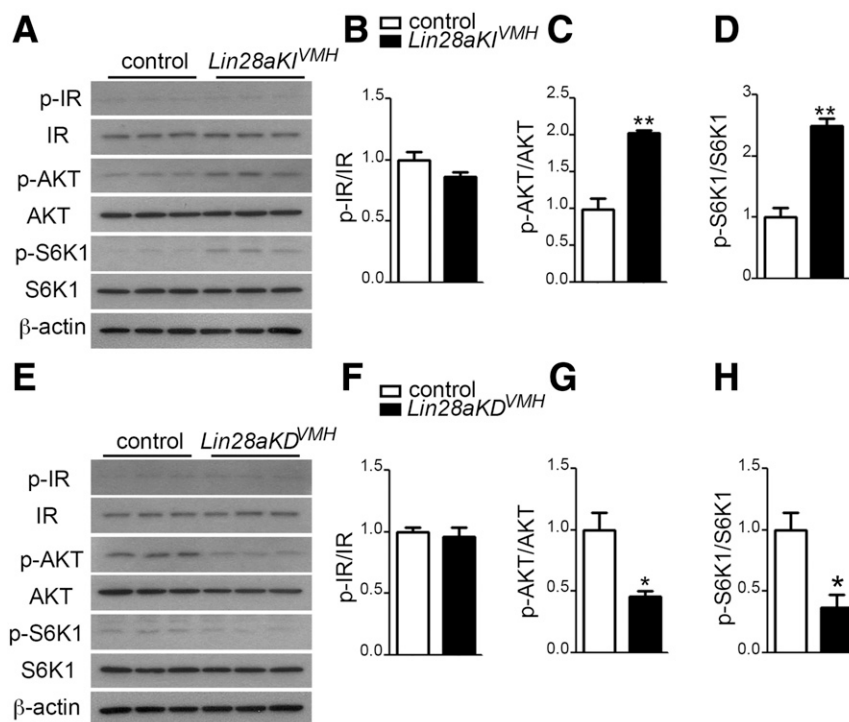

Figure 6—Lin28a affects AKT-mTOR pathways. A: Western blot images showing p-IR, total IR, p-AKT, total AKT, p-S6K1, total S6K1, and β-actin in VMH samples of control and Lin28aKI^{VMH} mice on an HFD (45%). B–D: Graphs showing the densitometry analyses of p-IR/IR (B), p-AKT/AKT (C), and p-S6K1/S6K1 (D) in the VMH of Lin28aKI^{VMH} mice and controls. E: Western blot images showing p-IR, total IR, p-AKT, total AKT, p-S6K1, total S6K1, and β-actin in VMH samples of control and Lin28aKD^{VMH} mice on an HFD (45%). F–H: Graphs showing the densitometry analyses of p-IR/IR (F), p-AKT/AKT (G), and p-S6K1/S6K1 (H) in the VMH of Lin28aKD^{VMH} mice and controls. n = 3 for all groups. Data represent the mean ± SEM. *P < 0.05; **P < 0.01.

were affected by changes in VMH Lin28a levels, we then analyzed VMH *Let-7* levels in both *Lin28aKI^{VMH}* and *Lin28aKD^{VMH}* mice and compared them with those of their respective controls. No differences in VMH *Let-7* levels were observed between either *Lin28aKI^{VMH}* mice and their controls (Fig. 7A–E) or *Lin28aKD^{VMH}* mice and their controls (Fig. 7F–J). Altogether, these results suggest that Lin28a-mediated AKT-mTOR activation is *Let-7* independent.

TBK-1 Mediates Lin28a-Induced AKT Activation, and Its Inhibition Impairs Glucose Metabolism

TBK-1, a serine/threonine kinase, has been shown to directly activate AKT (14–16). First, we assessed TBK-1 levels in the hypothalamus of mice exposed to either an SD or an HFD. Similar to Lin28a, hypothalami of DIO mice showed significantly greater levels of TBK-1 compared with those of SD mice (Fig. 8A and B). To determine whether Lin28a-induced AKT activation was mediated by TBK-1, we then assessed TBK-1 protein levels in the VMH of *Lin28aKI^{VMH}* and *Lin28aKD^{VMH}* mice compared with their respective controls. TBK-1 protein levels were upregulated in the *Lin28aKI^{VMH}* mice (Fig. 8C and D) while downregulated in the *Lin28aKD^{VMH}* mice (Fig. 8E and F)

compared with their respective controls. Similar to TBK-1 protein levels, VMH *TBK-1* mRNA levels were also significantly altered (Fig. 8G and I) in *Lin28aKI^{VMH}* and *Lin28aKD^{VMH}* mice compared with controls. On the other hand, mRNA levels of RICTOR, known as PI3K-dependent AKT kinase (17), were not affected (Fig. 8H and J). To further assess whether TBK-1 is a target of Lin28a, we next performed RIP using Lin28a antibody, followed by cDNA synthesis and quantitative PCR. *TBK-1* mRNA was approximately fourfold more enriched in the Lin28a immunoprecipitation samples compared with the levels in immunoprecipitation samples using a control antibody (IgG) (Fig. 8K and M). To assess the effect of selective VMH inhibition of TBK-1 on glucose metabolism, we injected the VMH of DIO control and *Lin28aKI^{VMH}* mice with BX795, a TBK-1 inhibitor, and 50 min later performed a GTT. Glucose administration in VMH-injected BX795 control mice induced a significant elevation of circulating glucose levels compared with that observed in VMH-injected vehicle mice (Fig. 8N). Similar results were obtained when BX795 was injected in the VMH of *Lin28aKI^{VMH}* mice (Fig. 8N). However, selective VMH inhibition of the PI3K-mTOR pathway using either LY294002 (Supplementary Fig. 7A and B) or rapamycin
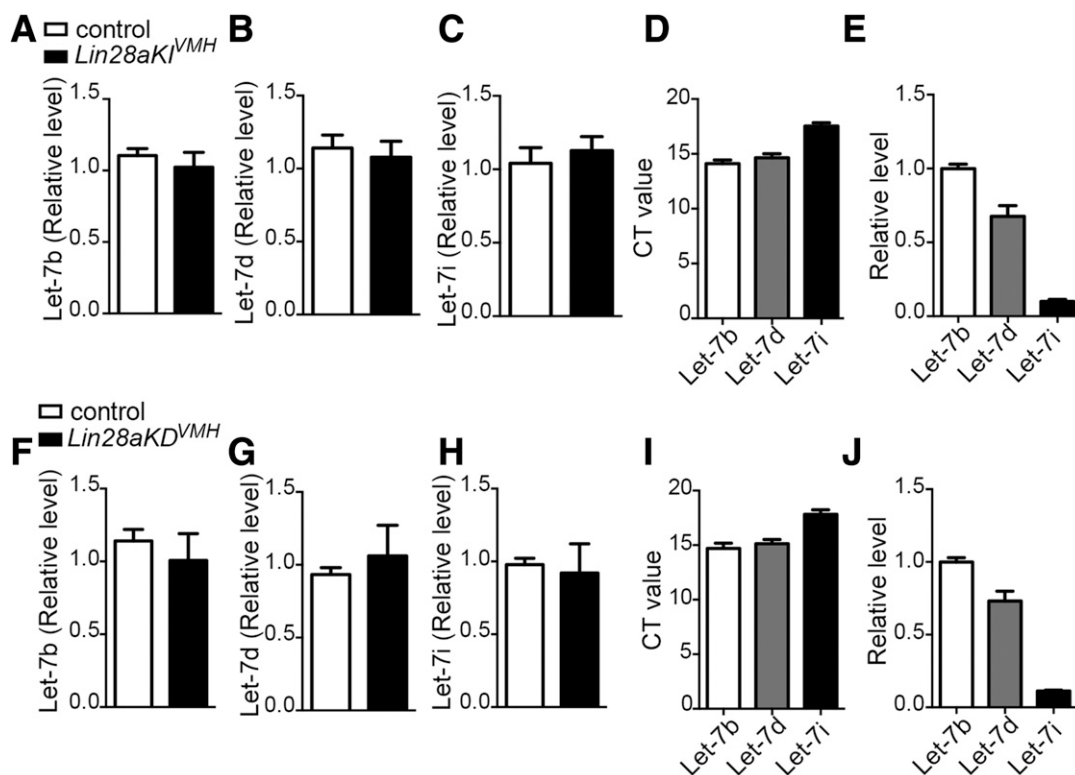

Figure 7—VMH Lin28a does not affect Let-7 levels. A–C: Real-time PCR for Let-7b (A), Let-7d (B), and Let-7i (C) in VMH samples of *Lin28aKI^{VMH}* mice and controls (n = 7 per group). D: Graph showing the cycle threshold (CT) values of Let-7b, Let-7d, and Let-7i in the VMH of *Lin28aKI^{VMH}* mice and controls (n = 7 per group). E: Graph showing the relative RNA levels of Let-7b, Let-7d, and Let-7i in the VMH of *Lin28aKI^{VMH}* mice and controls (n = 7 per group). F–H: Real-time PCR for Let-7b (F), Let-7d (G), and Let-7i (H) in VMH samples of *Lin28aKD^{VMH}* mice and controls (n = 5 per group). I: Graph showing the CT values of Let-7b, Let-7d, and Let-7i in the VMH of *Lin28aKD^{VMH}* mice and controls (n = 5 per group). J: Graph showing the relative RNA levels of Let-7b, Let-7d, and Let-7i in the VMH of *Lin28aKD^{VMH}* mice and controls (n = 5 per group). Data represent the mean ± SEM.
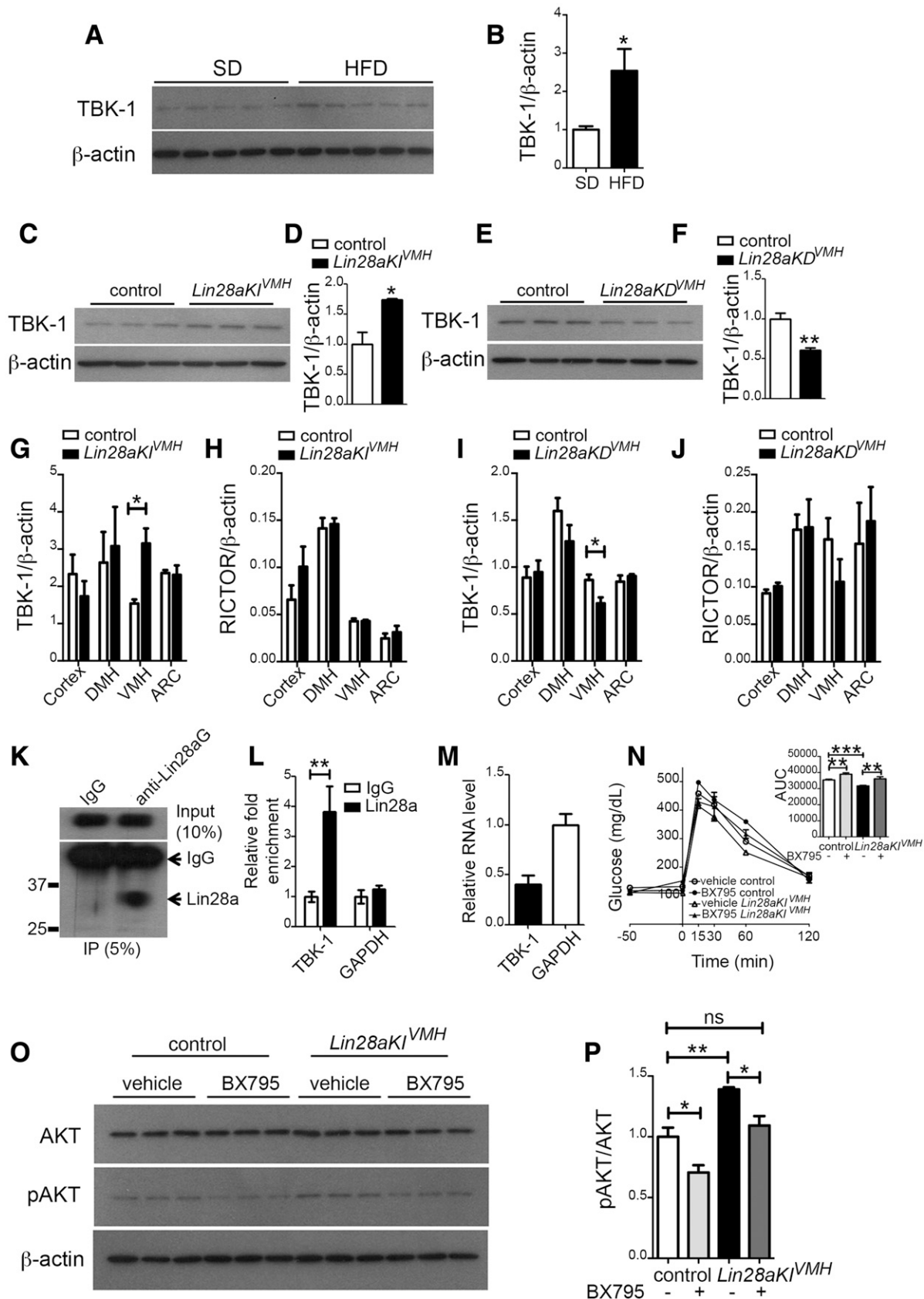
Figure 8—VMH Lin28a targets TBK-1 mRNA. *A* and *B*: Western blot images (*A*) and densitometry analysis (*B*) of TBK-1 expression levels in the hypothalamus of mice exposed to either SD (*n* = 5) or 8 weeks of HFD (*n* = 5). *C* and *D*: Western blot images (*C*) and densitometry analysis (*D*) of TBK-1 expression levels in the VMH of *Lin28aKI^VMH* mice and controls on an HFD for 8 weeks (*n* = 3 per group). *E* and *F*: Western blot images (*E*) and densitometry analysis (*F*) of TBK-1 expression levels in the VMH of *Lin28aKD^VMH* mice and controls on an HFD for 8 weeks (*n* = 3 per group).

(Supplementary Fig. 7C and D) in DIO mice showed no effect on glucose metabolism. Finally, to determine the effect of TBK-1 inhibition on AKT activation we assessed p-AKT/AKT after VMH injection of either BX795 or vehicle in DIO control and *Lin28aKI*^{VMH} mice. In control mice, BX795 significantly decreased pAKT/AKT compared with vehicle-injected mice (Fig. 8O and P). Similarly, in *Lin28a-KI*^{VMH} mice, BX795 also decreased pAKT/AKT to reach levels similar to those observed in vehicle-injected DIO control mice (Fig. 8O and P). Taken together, these results indicate that TBK-1 mediates Lin28a-induced AKT activation and that TBK-1 inhibition in the VMH of DIO mice impairs their response to a glucose load.

DISCUSSION

Our study shows that Lin28a, an RNA-binding protein highly expressed in the hypothalamus compared with peripheral organs, is regulated by the metabolic state. Specifically, we show that hypothalamic Lin28a expression levels correlate with positive energy metabolism. In the fasting condition, Lin28a expression levels were significantly lower compared with the fed state, while in HFD feeding, Lin28a levels were increased compared with SD feeding. To further determine the role of Lin28a, we then generated mouse models with either selective overexpression or downregulation of Lin28a in the VMH, which is involved in the regulation of energy and glucose homeostasis. Interestingly, Lin28a expression in the VMH did not influence body weight or composition when mice were exposed to either SD or HFD. However, we observed a positive correlation between Lin28a expression levels and glucose homeostasis in mice fed an HFD. Lin28a overexpression in the VMH induced a significant improvement in glucose metabolism, while Lin28a downregulation during HFD was detrimental. The apparent discrepancy between the elevated hypothalamic Lin28a levels in DIO mice and the overexpression mice could represent the need to increase Lin28a to improve glucose metabolism when challenged with an HFD. To assess the intracellular signaling pathway mediating these effects on glucose metabolism, we studied the well-characterized IR-PI3K-AKT-mTOR pathway in the VMH. While no significant differences in IR phosphorylation levels were found, VMH AKT and mTOR activation levels were significantly affected. Interestingly, Lin28-induced activation of AKT and mTOR was not associated with changes in *Let*-7 expression. Lin28a was found to interact and regulate TBK-1, a kinase that phosphorylates and activates AKT (14–16). Selective inhibition of TBK-1, but not PI3K or mTOR, in the VMH significantly impaired glucose metabolism in HFD-fed mice and reduced AKT activation. Altogether, our study demonstrated a physiological role for central Lin28a in the regulation of peripheral glucose metabolism mediated by TBK-1.

The Lin28a/*Let*-7 axis has been shown to regulate many physiological processes, including cell proliferation and neurogenesis (2,18,19). More recently, two independent groups have shown that the Lin28a/*Let*-7 axis also plays a role in the regulation of glucose homeostasis and insulin sensitivity (3,4). Whole-body Lin28a transgenic mice showed improvement in glucose clearance and insulin sensitivity that was associated with reduced *Let*-7 expression in the muscle (4). When *Let*-7 was globally overexpressed, impaired glucose tolerance was observed (4). Interestingly, selective deletion of Lin28a in the muscle, using the *Lin28a*$^{fl/fl}$-*Myf5-cre* mouse model, was not associated with changes in *Let*-7 expression levels (5). In this study, only when Lin28a was overexpressed in vitro in C2C12 cells, a reduction of *Let*-7 levels was observed. Although these studies (3–5) show that Lin28a regulates glucose metabolism, the mechanism of action seems to be mediated only in part by *Let*-7. Our study, while further supporting a physiological role for hypothalamic Lin28a in the control of glucose homeostasis, suggests that a hypothalamic Lin28a effect on glucose metabolism is not mediated by changes in *Let*-7 levels. In support of a *Let*-7–independent mechanism of action, Lin28a-induced mTOR pathway activation has been shown to regulate neural progenitor cell proliferation without affecting *Let*-7 levels (20). As an RNA-binding protein, Lin28a can indeed directly affect various mRNA targets without altering *Let*-7 miRNA levels (21,22). We found that in the hypothalamus Lin28a targets *TBK-1* mRNA, a kinase that directly activates the AKT pathway independently from insulin-PI3K-mTOR signaling (14–16). Similar to previous data (21,22), we found that, in the VMH, Lin28a regulates peripheral glucose metabolism by directly controlling *TBK-1* mRNA expression. In further support of this, RICTOR expression, a PI3K-dependent AKT kinase and also one of the mRNA targeted by *Let*-7 (4), was not affected in our animal

---

G: Graph showing real-time PCR for TBK-1 in the cortex, DMH, VMH, and hypothalamic ARC of *Lin28aKI*^{VMH} mice and controls on an HFD (for 8 weeks). *H*: Graph showing real-time PCR for RICTOR in the cortex, DMH, VMH, and hypothalamic ARC of *Lin28aKI*^{VMH} mice and controls on an HFD (for 8 weeks). *I*: Graph showing real-time PCR for TBK-1 in the cortex, DMH, VMH, and hypothalamic ARC of *Lin28aKD*^{VMH} mice and controls on an HFD (for 8 weeks). *J*: Graph showing real-time PCR for RICTOR in the cortex, DMH, VMH, and hypothalamic ARC of *Lin28aKD*^{VMH} mice and controls on an HFD (for 8 weeks). *K*: Immunoprecipitation using polyclonal anti-Lin28a, followed by Western blot analysis. Ten percent input was loaded in the upper panel. Five percent immunoprecipitated (IP) hypothalamic samples were loaded in the lower panel. *L*: RIP with rabbit polyclonal anti-Lin28a or preimmune IgGs from hypothalamic extracts. RNA levels in immunoprecipitates were determined using reverse transcription and quantitative PCR. Levels of TBK-1 and GAPDH mRNA are presented as fold enrichment in anti-Lin28a relative to IgG immunoprecipitates. *M*: Relative RNA levels of TBK-1 and GAPDH in hypothalamic samples ($n = 4$ mice). *N*: Graph showing the results of a GTT 50 min after the VMH of HFD-fed control and *Lin28aKI*^{VMH} mice ($n = 6$ per group) was injected with either vehicle (0.1% DMSO in saline) or BX795 (10 ng/site). AUC, area under the curve. *O* and *P*: Western blot images (*O*) and densitometry analysis (*P*) of AKT (total) and pAKT expression levels in the VMH of *Lin28aKI*^{VMH} mice and controls on an HFD for 8 weeks ($n = 3$ per group) injected either with BX795 (10 ng/site) or with vehicle control. Data represent the mean ± SEM. *$P < 0.05$; **$P < 0.01$; ***$P < 0.001$. ns, not significant.

models. Furthermore, injections of either PI3K or mTOR inhibitors directly in the VMH of DIO mice did not affect peripheral glucose metabolism, suggesting that the IR-PI3K pathway activation in the VMH is not involved in the control of peripheral glucose metabolism. In agreement with this, Klöckener et al. (23) reported that selective deletion of IR in SF1 neurons of the VMH does not directly regulate peripheral glucose metabolism.

The regulation of Lin28a expression is still not well defined. Interestingly, similar to the VMH-selective Lin28a overexpression mice, mice injected in the VMH with either leptin or melanotan II (MTII), a melanocortin receptor agonist, showed a preferential increase in glucose uptake in the muscle and the heart (24). This raises the possibility that a possible link between circulating leptin levels and Lin28a expression in the VMH may exists. Consistent with this, we found that in the fasted state, characterized by a decline of leptin levels, Lin28a expression in the VMH is significantly decreased compared with that in the fed state. The possible role of leptin in the regulation of Lin28a expression warrants future studies.

In summary, our studies revealed a physiological role for Lin28a in the VMH in the regulation of glucose homeostasis. In the VMH, Lin28a regulation of the insulin pathway was associated not with changes in *Let-7* but, rather, with changes in TBK-1 expression and increased excitability of VMH neurons. This pathway may represent a mechanism that functions to alter peripheral insulin sensitivity in response to changes in circulating glucose levels.

Duality of Interest. No potential conflicts of interest relevant to this article were reported.
Author Contributions. J.D.K. performed all the experiments and analyzed data related to Figs. 1–4, 6, and 8. C.T. performed experiments related to Fig. 5. C.M.R. and C.F.-H. performed experiments and analyzed data related to Fig. 7. S.D. conceived the study, designed the experiments, and analyzed data. S.D. wrote the manuscript. S.D. is the guarantor of this work and, as such, had full access to all the data in the study and takes responsibility for the integrity of the data and the accuracy of the data analysis.

References

1. Viswanathan SR, Daley GQ, Gregory RI. Selective blockade of microRNA processing by Lin28. Science 2008;320:97–100

2. Thornton JE, Gregory RI. How does Lin28 let-7 control development and disease? Trends Cell Biol 2012;22:474–482

3. Frost RJ, Olson EN. Control of glucose homeostasis and insulin sensitivity by the Let-7 family of microRNAs. Proc Natl Acad Sci U S A 2011;108:21075–21080

4. Zhu H, Shah S, Shyh-Chang N, et al. Lin28a transgenic mice manifest size and puberty phenotypes identified in human genetic association studies. Nat Genet 2010;42:626–630

5. Zhu H, Shyh-Chang N, Segre AV, et al. The Lin28/let-7 axis regulates glucose metabolism. Cell 2011;147:81–94

6. Grayson BE, Seeley RJ, Sandoval DA. Wired on sugar: the role of the CNS in the regulation of glucose homeostasis. Nat Rev Neurosci 2013;14:24–37

7. Seoane-Collazo P, Ferno J, Gonzalez F, et al. Hypothalamic-autonomic control of energy homeostasis. Endocrine 2015;50:276–291

8. Kim JD, Toda C, D'Agostino G, et al. Hypothalamic prolyl endopeptidase (PREP) regulates pancreatic insulin and glucagon secretion in mice. Proc Natl Acad Sci U S A 2014;111:11876–11881

9. Routh VH. Glucose sensing neurons in the ventromedial hypothalamus. Sensors (Basel) 2010;10:9002–9025

10. Fioramonti X, Song Z, Vazirani RP, Beuve A, Routh VH. Hypothalamic nitric oxide in hypoglycemia detection and counterregulation: a two-edged sword. Antioxid Redox Signal 2011;14:505–517

11. Choi YH, Fujikawa T, Lee J, Reuter A, Kim KW. Revisiting the ventral medial nucleus of the hypothalamus: the roles of SF-1 neurons in energy homeostasis. Front Neurosci 2013;7:71

12. White MF. Mechanism of insulin action. In *Textbook of Diabetes.* Holt RIG, Cockram CS, Flyvbjerg A, Goldstein BJ, Eds. Wiley-Blackwell, Chichester, U.K., 2017, p. 114–132

13. Toda C, Kim JD, Impellizzeri D, Cuzzocrea S, Liu ZW, Diano S. UCP2 regulates mitochondrial fission and ventromedial nucleus control of glucose responsiveness. Cell 2016;164:872–883

14. Joung SM, Park ZY, Rani S, Takeuchi O, Akira S, Lee JY. Akt contributes to activation of the TRIF-dependent signaling pathways of TLRs by interacting with TANK-binding kinase 1. J Immunol 2011;186:499–507

15. Xie X, Zhang D, Zhao B, et al. IkappaB kinase epsilon and TANK-binding kinase 1 activate AKT by direct phosphorylation. Proc Natl Acad Sci U S A 2011;108:6474–6479

16. Ou YH, Torres M, Ram R, et al. TBK1 directly engages Akt/PKB survival signaling to support oncogenic transformation. Mol Cell 2011;41:458–470

17. Sarbassov DD, Guertin DA, Ali SM, Sabatini DM. Phosphorylation and regulation of Akt/PKB by the rictor-mTOR complex. Science 2005;307:1098–1101

18. Cimadamore F, Amador-Arjona A, Chen C, Huang CT, Terskikh AV. SOX2-LIN28/let-7 pathway regulates proliferation and neurogenesis in neural precursors. Proc Natl Acad Sci U S A 2013;110:E3017–E3026

19. Shyh-Chang N, Daley GQ. Lin28: primal regulator of growth and metabolism in stem cells. Cell Stem Cell 2013;12:395–406

20. Yang M, Yang SL, Herrlinger S, et al. Lin28 promotes the proliferative capacity of neural progenitor cells in brain development. Development 2015;142:1616–1627

21. Xu B, Zhang K, Huang Y. Lin28 modulates cell growth and associates with a subset of cell cycle regulator mRNAs in mouse embryonic stem cells. RNA 2009;15:357–361

22. Peng S, Chen LL, Lei XX, et al. Genome-wide studies reveal that Lin28 enhances the translation of genes important for growth and survival of human embryonic stem cells. Stem Cells 2011;29:496–504

23. Klöckener T, Hess S, Belgardt BF, et al. High-fat feeding promotes obesity via insulin receptor/PI3K-dependent inhibition of SF-1 VMH neurons. Nat Neurosci 2011;14:911–918

24. Toda C, Shiuchi T, Lee S, et al. Distinct effects of leptin and a melanocortin receptor agonist injected into medial hypothalamic nuclei on glucose uptake in peripheral tissues. Diabetes 2009;58:2757–2765